Chinese Chemical Letters 34 (2023) 108245

Contents lists available at ScienceDirect

Chinese Chemical Letters

journal homepage: www.elsevier.com/locate/cclet

Enhanced Li^+ migration in solid polymer electrolyte driven by anion-containing polymer-chains

Xingyi Zhang[a,b,1], Modeste Venin Mendieev Nitou[a,b,1], Wenjun Li[a,b], Zhao Wan[b], Longfei Liu[b], Zhaohui Luo[c], Sohail Muhammad[a,b], Wu Qin[d], Liang An[e], Yinghua Niu[a,b,f,*], Weiqiang Lv[a,b,*]

[a] Yangtze Delta Region Institute (Huzhou), University of Electronic Science and Technology of China, Huzhou 313001, China
[b] School of physics, University of electronic Science and Technology of China, Chengdu 611731, China
[c] X-Energy Systems Co., Ltd., Jiaxing 314000, China
[d] National Engineering Laboratory for Biomass Power Generation Equipment, School of Renewable Energy Engineering, North China Electric Power University, Beijing 102206, China
[e] Department of Mechanical Engineering, the Hong Kong Polytechnic University, Hong Kong, China
[f] Zhejiang Humo Polishing Grinder Manufacture Co., Ltd., Huzhou 313012, China

ARTICLE INFO

Article history:
Received 12 December 2022
Revised 17 January 2023
Accepted 16 February 2023
Available online 19 February 2023

Keywords:
Solid polymer electrolyte
Lithiated perfluorinated sulfonic acid
Polyvinylidene fluoride
Solid-state battery
Anion containing polymer

ABSTRACT

Li-ion batteries with solid polymer electrolytes (SPEs) are safer than conventional liquid electrolytes due to the absence of highly flammable liquid electrolytes. However, their performance is limited by the poor Li^+ transport in SPEs at room temperature. Anion-containing polymer-chains incorporated SPEs (ASPEs) are therefore developed to enhance Li^+ diffusion kinetics. Herein, we propose a novel and feasible strategy to incorporate the anion-containing polymer-chains, such as lithiated perfluorinated sulfonic acid (PFSA), into polyvinylidene fluoride (PVDF) polymer-based SPEs. The immobile anion groups from the PFSA-chains impede the migration of mobile anion groups dissociated from the Li salt. The transference number is thus raised from ~0.3 to 0.52 with the introduction of anion-containing polymer-chains into SPEs. The electrostatic repulsion among anion-containing chains also reduces the close chain stacking and brings 159% increase in the ionic conductivity to 0.83×10^{-3} S/cm at 30 °C in contrast with the pure PVDF-based SPE. In addition, $LiFeO_4$/Li batteries with ASPEs exhibit 55% capacity boost at 0.5 C in contrast to the capacity of batteries with pure-PVDF SPEs, and also offer more than 1000 charge/discharge cycles. Our research findings potentially offer a facile strategy to design thermal stable SPEs with superior Li^+ transport behaviors towards developing high-performance SPEs-based batteries.

Li-ion batteries (LIBs), due to their high power density and energy density have been widely employed in portable electronic devices, grid energy storage, and electric vehicles [1]. However, traditional LIBs generally consist of organic liquid electrolytes, which makes LIBs risky in terms of thermal instability, liquid leakage fire, and even explosion. Solid-state LIBs (SSLIBs) can largely solve these safety issues [2,3]. The electrolyte of SSLIBs could be divided into ceramic electrolyte and solid polymer electrolytes (SPEs) [4]. The electrode/electrolyte interface contact and stability are enormous challenges for ceramic electrolyte-based LIBs [5]. SPEs, on the other hand, are flexible and possess the advantage of forming a well-contacted and stable electrode/electrolyte interface [6]. The most used solid polymer electrolytes are poly(ethylene oxide) (PEO) and its various derivatives [5,7]. One of the main challenges of SPEs is the low Li-ion conductivity (σ_{Li^+}) and transference number (t_{Li^+}) at room temperature [8]. For the most used PEO based SPEs, the ionic conductivity is at the order of 10^{-3} S/cm at 60~100 °C, whereas it decreases fast below 60 °C (*e.g.*, 2.1×10^{-6} S/cm at 20 °C) due to the PEO-chain crystalline [8–10]. Moreover, the PEO-based SPEs have poor mechanical strength and thermostability [11]. Poly(vinylidene fluoride) (PVDF) and its derivatives show excellent electrochemical stability [12] and the strong electron-withdrawing group (–C–F) can contribute to the dissolution and dissociation of alkali metal salts for high carrier concentrations [13]. However, PVDF and its derivatives cannot provide an excellent Li-ion conductivity in a dried state due to the restricted polymer-chain motion arising from the high degree of crystallinity of PVDF-based polymers [7,14]. Furthermore, the conventional SPEs

* Corresponding authors.
E-mail addresses: yh_niu@aliyun.com (Y. Niu), eselwq@uestc.edu.cn (W. Lv).
[1] These authors contributed equally to this work.

https://doi.org/10.1016/j.cclet.2023.108245
1001-8417/

formed by blending Li salt [15,16] (*e.g.*, Li[$(CF_3SO_2)_2N$ (LiTFSI), $LiClO_4$, $LiCF_3SO_3$)] with polymers are dual-ion conductors [16]. Li-ions and anions move in the opposite direction and accumulate at the electrode/electrolyte interfaces, the interfacial charge accumulation and anion concentration gradient resist Li^+ migration, resulting in severe cell polarization [17,18]. Single-ion conducting polymer electrolytes with anions bounded to the long chain of polymers own very high transference number but typically low ionic conductivity at room temperature [17,19]. To increase the low transference number and Li-ion conductivity of SPE, incorporating anion-containing polymer-chains with the characteristic of single-ion conductors into SPEs can form anion-containing polymer blend SPEs (ASPEs). The immobilized anion groups from the anion-containing polymer can restrict the motion of the dissociative anion from the Li salts. Meanwhile, the charged anion-containing polymer-chains may reduce the close stacking of polymer-chains, facilitating the polymer segmental motion and therefore promoting the Li^+ migration.

In this work, the anion-containing polymer chains, perfluorinated sulfonic acid resin (PFSA, with $-SO_3^-$ group), was incorporated into PVDF-based SPEs to enhance the Li^+ transport kinetics of SPEs. The perfluorinated backbone provides high chemical and thermal stability while the sulfonic groups are bound to the side chains of the polymer [20]. A schematic diagram of a solid-state LIB in Fig. 1a includes a PVDF-PFSA ASPE LIB, a current collector, a Li metal anode, a $LiFePO_4$ cathode, and a carbon-coated allium foil. The molecule structure of PFSA in Fig. 1b shows a perfluoro main chain and a $-SO_3$ anion-containing side chain. Figs. 1c and d demonstrate the Li^+ and $TFSI^-$ transport behavior during the charge/discharge process in battery with PVDF SPE and PVDF-PFSA ASPE, respectively. In pure PVDF SPEs, both Li^+ and $TFSI^-$ diffuse toward opposite directions, causing charge accumulation at the electrode/SPE interface with large polarization. In ASPE, the motion of $TFSI^-$ driven by polymer segment motion is restricted due to the electrostatic repulsion between negatively charged $TFSI^-$ and the anion-containing groups. The reduced interfacial polarization brings uniform Li^+ deposition on Li metal, capable of suppressing Li dendrite growth. The scanning electron microscopy (SEM) images in Figs. 1e and f show that the PVDF-based SPE exhibits a worm-like structure with pores on the surface, whereas PVDF-PFSA-based ASPE indicates a non-porous flake-like structure, indicating the significant impact of the anion-containing PFSA-chains on polymer-chain stacking. The inserted optical image shows that the SPE turns from semi-transparent to opaque when incorporating anion-containing chains into SPEs, suggesting a reduction in crystallinity. The cross-section test result in Fig. S1 (Supporting information) shows that the thickness of the SPEs is ~50 μm. The X-ray diffraction (XRD) patterns in Fig. S2a (Supporting information) shows that the intensities of the peaks associated with PVDF decrease with increasing PFSA content in the PVDF-PFSA ASPEs, indicating the decreased crystallinity of the ASPEs. The Fourier transform infrared (FTIR) spectra in Fig. S2b (Supporting information) show that no new peak appears in the blended PVDF-PFSA ASPEs, demonstrating that no obvious reaction or bonding occurs among PVDF, PFSA and LiTFSI.

The Li^+ migration characterization of PVDF SPEs and PVDF-PFSA ASPEs is shown in Fig. 2. As shown in Fig. 2a, at a fixed temperature, the ionic conductivity of the SPEs increases with increasing PFSA contents. The Li-ion conductivity of ASPEs with 40% PFSA is 0.83×10^{-3} S/cm at 30 °C, which is more than 2.5 times that of pure PVDF-based SPEs (0.32×10^{-3} S/cm). Further increasing PFSA content in the SPEs causes abrupt mechanical failure of the ASPEs, as shown in Fig. S3 (Supporting information). The activation energy for Li-ion diffusion can be obtained from the slope of the fitted line over $\log\sigma \sim 1/T$ data according to the Arrhenius equation. After incorporating 40% PFSA into the PVDF based electrolytes, the activation energy of Li-ion diffusion reduces from ~0.35 eV to ~0.22 eV. The increased pre-exponential factor affected by the carrier concentration can also promote the ionic conduction SPEs since the lithiated PFSA bring more Li-ions in ASPEs [21].

Fig. 2b shows that the Li^+ transference number increases from 0.30 to 0.52 with increasing the ratio of PFSA from 0 to 40%, verifying that the anion-containing chains impede the migration of $TFSI^-$ anions. Different current densities are applied to symmetrical Li/Li

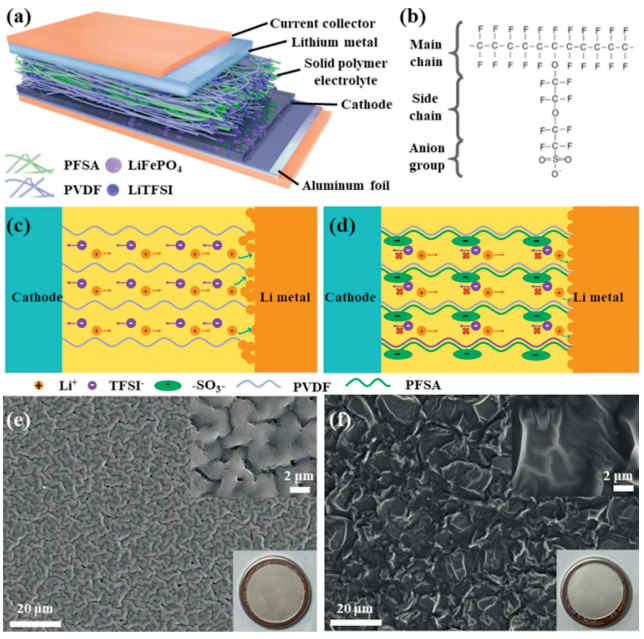

Fig. 1. The characterization of the PVDF-PFSA/LiTFSI SPEs. (a) The schematic diagram of a solid-state LIB with the PVDF-PFSA ASPE, current collector, Li metal anode, $LiFePO_4$ cathode, and carbon-coated aluminum foil. (b) The molecular structure of PFSA with the perfluoro main chain and the $-SO_3$ anion-containing side chain. Schematics of Li^+ and $TFSI^+$ transport and Li^+ deposition during the charge/discharge in batteries with (c) PVDF SPE and (d) PVDF-PFSA ASPE. The SEM image of (e) PVDF SPE and (f) PVDF-PFSA ASPE. Insets are the enlarged SEM images (right top) and optical photos (right bottom) of solid electrolytes.

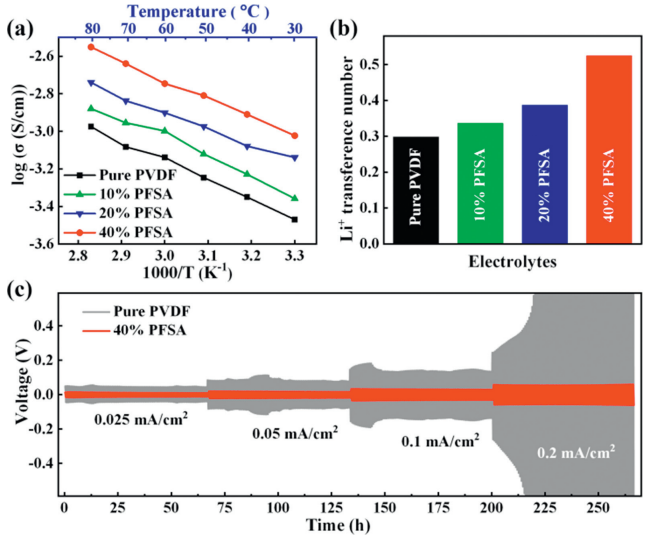

Fig. 2. The characterization of Li^+ migration in PFSA/PVDF SPEs. (a) Ionic conductivity measurements with linear fitting. (b) Li-ions transference number of 40% PFSA, 20% PFSA, 10% PFSA and PVDF SPEs at room temperature. (c) Voltage-time profiles of the Li/Li symmetric cell at various current densities over long cycles and at 30 °C.

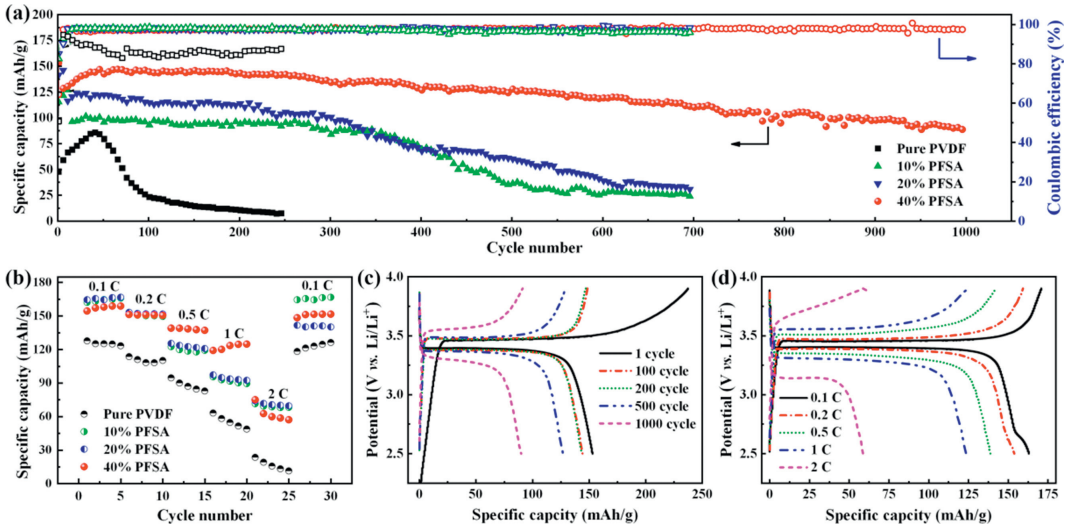

Fig. 3. Electrochemical performance of the $LiFePO_4$/Li cells at 30 °C. (a) Cycling performance and columbic efficiency for cells with 40% PFSA, 20% PFSA, 10% PFSA, and pure PVDF SPEs (The first cycle is at 0.1 C, the others are at 0.5 C). (b) Rate performance of cells with different SPEs at 0.1, 0.2, 0.5, 1 and 2 C. Charge/discharge voltage profiles of cells with the 40% PFSA ASPE (c) at different cycles and (d) at different C-rates.

batteries with different types of SPEs (Fig. 2c). At 0.025 mA/cm^2, the polarization voltage of the Li/Li symmetric cell is ~0.02 V for the ASPE with 40% PFSA, only one third of that for the pure PVDF SPE. As the current density increases from 0.025 mA/cm^2 to 0.2 mA/cm^2, the polarization voltage for the ASPE with 40% PFSA increases from ~0.02 V to 0.05 V, whereas the polarization voltage for the pure PVDF SPE increases from ~0.06 V to more than 0.3 V. The ASPEs with 40% PFSA shows much smaller polarization within ~270 h test at different current densities as compared with the pure PVDF SPE, indicating that the anion containing PFSA-chains promotes the Li^+ transport kinetics with faster and more uniform Li^+ flux for the suppression of Li metal dendrite growth. The thermogravimetric (TG)/differential scanning calorimetry (DSC) curves in Fig. S4 (Supporting information) and the infrared thermography images (Fig. S5 in Supporting information) of pure PVDF and PVDF blend with 40% PFSA indicate that incorporating PSFA into PVDF based SPEs can enhance the thermal stability.

Fig. 3a shows the long-term cycle performance of $LiFePO_4$/Li metal half cells and the corresponding Coulombic efficiency (CE) of different ratios of PFSA-PVDF ASPEs at 0.5 C and 30 °C. It is noted that the first to third cycles were charged/discharged at 0.1 C. There is a capacity rise during the first 50 cycles for all the cells. This phenomenon can also be observed in other works [22–24]. The $LiFePO_4$/Li cells deliver capacities of 80.8 mAh/g for the pure PVDF SPE, 96.0 mAh/g for the 10% PFSA ASPE, 122.4 mAh/g for the 20% PFSA ASPE and 146.8 mAh/g for the 40% PFSA ASPE at the 50th cycle. From the 50th cycle to the 100th cycle, the capacity retention for the pure PVDF SPE is only 27.8%, whereas the capacity retention is 96% for the 10% PFSA ASPE, 93.7% for the 20% PFSA ASPE and nearly 100% for the 40% PFSA ASPE. Before the 200th cycle, the cells with 10%-40% PFSA ASPEs show rather stable capacities, and obvious capacity fading occurs after 300 cycles. The specific capacity for cells with 10%~20% PFSA SPEs is below 30 mAh/g after 700 cycles, whereas the cells with 40% PFSA delivers a discharge capacity of 89 mAh/g at the 1000th cycle with a capacity retention of ~59%, and the CE is close to 100% after 1000 cycles. Fig. 3b shows the rate performance of different ratios of PFSA-PVDF ASPEs. The reversible capacities of 164, 150, 138, 124 and 60 mAh/g were obtained at 0.1, 0.2, 0.5, 1 and 2 C for the 40% PFSA. The reversible capacity reaches 151 mAh/g when the current density returns to 0.1 C after being cycled 30 times. In contrast, the pure PVDF SPE delivers a much lower discharge capacity of 11 mAh/g at 2 C. Fig. 3c shows the charge/discharge curves during the selected cycles. The specific discharge capacities of 40% PFSA are 153, 144, 143, 127 and 89 mAh/g after the 1st, 100th, 200th, 500th and 1000th cycles, respectively. The voltage hysteresis between the charge and discharge plateaus is small before the 500th cycle. Fig. 3d presents the charge/discharge curves at 0.1-2 C of 40% PFSA ASPEs. Flat charge and discharge plateaus is observed before 1 C, but there is a considerable voltage hysteresis between the charge and discharge plateaus at 2 C.

Fig. 4 shows the optimized structures and the adsorption energies between different components in the PFSA-PVDF SPE by

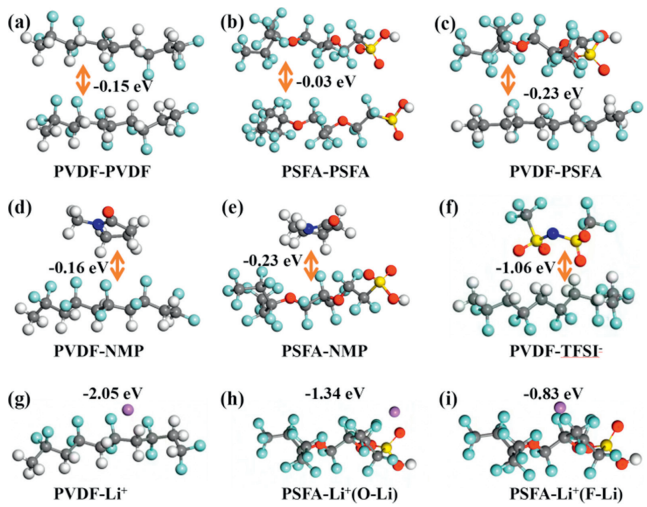

Fig. 4. DFT calculation optimized structures and the adsorption energies between different components in the PFSA-PVDF SPE: (a) The interaction between two PVDF polymer chains; (b) the interaction between two PFSA polymer-chains; (c) the interaction between the PVDF chain and the PFSA-chain; (d) the interaction between the PVDF chain and the residual plasticizer NMP; (e) the interaction between the PFSA-chain and the residual plasticizer NMP; (f) the interaction between the PVDF-chain and $TFSI^-$; (g) the interaction between the PVDF chain and Li^+; (h) the interaction between the PVDF sulfonic group and Li^+; and (i) the interaction between the PFSA perfluorinated-chain and Li^+. The balls with different colors represent different atoms: White balls for hydrogen, grey balls for carbon, cyan balls for florine, red balls for oxygen, yellow balls for sulfur, purple balls for lithium, blue balls for nitrogen.

density functional theory (DFT) calculations. By comparing the adsorption energy between PVDF-polymer chains and PFSA polymer-chains (Figs. 4a–c), the adsorption energy between PVDF and PFSA-chain is larger than the adsorption energies between two PVDF-chains and between two PFSA-chains, facilitating the formation of a highly uniform PVDF-PFSA blend. Figs. 4d and e show that the interaction between PFSA and the residual plasticizer *N*-methyl pyrrolidone (NMP) is more significant than that between PVDF and NMP. Due to the strong affiliation of the PVDF-based electrolyte with low content of solvent NMP, NMP cannot be eliminated till 80 °C in vacuum, which is different from the PVDF-based electrolytes with high contents of solvent as gel polymer electrolytes (GPEs). The residual solvent functions as a plasticizer, and can dramatically enhance the ionic conductivity and amorphicity of the polymer matrix [22–24]. Fig. 4f shows that the adsorption energy between the PVDF chains and the anion $TFSI^-$ is as high as 1.06 eV. Considering the strong repulsion between the negatively charged sulfonic group in PFSA and the negatively-charged $TFSI^-$, significantly enhanced immobilization of $TFSI^-$ in PFSA-PVDF SPE (as compared with pure PVDF SPE) can be achieved. This is why the addition of PFSA into the PVDF-based SPE can dramatically enlarge the transference number of the SPE. By comparing the interaction between Li^+ and the polymer-chains (Figs. 4g–i), it is found that the interaction energy between the PFSA perfluorinated-chain and Li^+ is 0.85 eV, which is lower than the interaction of the both PVDF chain and the PFSA sulfonic group with Li^+, indicating that the PFSA perfluorinated-chain exhibits reduced immobilization to Li^+ motion, permitting the Li^+ conduction in the SPEs.

In summary, incorporating anion-containing PFSA-chains into PVDF-based SPEs significantly increases the ionic conductivity and transference number of ASPEs. The ionic conductivity number reaches 0.83×10^{-3} S/cm at 30 °C for the ASPE with 40% PFSA, which is about 2.5 times higher than that of pure PVDF-based SPE. The transference number also increases from 0.28 to 0.52 as the content of PFSA varies from 0 to 40% in the SPEs. The reduced crystallinity by the strong intra-chain electrostatic repulsion and the restriction of anion mobility arising from the electrostatic repulsion between the immobile anion groups on the polymer chain and the anions from Li salt contributes to the improvement of Li conduction and transference number. The $LiFePO_4$/Li batteries with the 40% PFSA ASPEs exhibit significantly improved cycling performance (the CE is close to 100% after 1000 cycles) and rate performance (60 mAh/g at 2 C) compared with batteries having pure PVDF-based SPEs (11 mAh/g at 2 C). Our work indicates that incorporating anion-containing polymers into SPEs is a versatile strategy to construct highly Li^+ conductive SPEs for high-performance LIBs.

Declaration of competing interest

No conflict of interest exists in the submission of this manuscript, and the manuscript is approved by all authors for publication. I would like to declare on behalf of my co-authors that the work described was original research that has not been published previously, and not under consideration for publication elsewhere, in whole or in part. All the authors have approved this manuscript.

Acknowledgments

This work was supported by the National Natural Science Foundation of China (Nos. 51972043 and 52102212), the Sichuan-Hong Kong Collaborative Research Fund (No. 2021YFH0184), the Foundation of Yangtze Delta Region Institute (Huzhou) of UESTC, China (Nos. U03210010 and U03210028) and Huzhou Science and Technology Special Representative Project (No. 2021KT54).

Supplementary materials

Supplementary material associated with this article can be found, in the online version, at doi:10.1016/j.cclet.2023.108245.

References

[1] L. Lu, X. Han, J. Li, J. Hua, M. Ouyang, J. Power Source 226 (2013) 272–288.
[2] R. Chen, Q. Li, X. Yu, L. Chen, H. Li, Chem. Rev. 120 (2020) 6820–6877.
[3] R.P. Doyle, X. Chen, M. Macrae, et al., Macromolecules 47 (2014) 3401–3408.
[4] C.L. Yan, Rare Metal 39 (2020) 458–459.
[5] N. Meng, F. Lian, G. Cui, Small 17 (2021) e2005762.
[6] W. Kou, Y. Zhang, W. Wu, et al., Green Energy Environ. (2022), doi:10.1016/j.gee.2022.05.002.
[7] T.K.L. Nguyen, G. Lopez, C. Iojoiu, R. Bouchet, B. Ameduri, J. Power Source 498 (2021) 229920.
[8] J. Zhang, J. Zhao, L. Yue, et al., Adv. Energy Mater. 5 (2015) 1501082.
[9] C. Yang, K. Fu, Y. Zhang, E. Hitz, L. Hu, Adv. Mater. 29 (2017) 1701169.
[10] Z. Xue, D. He, X. Xie, J. Mater. Chem. A 3 (2015) 19218–19253.
[11] Y.N. Liu, Z. Xiao, W.K. Zhang, et al., Rare Metal 41 (2022) 3762–3773.
[12] A.L. Chen, N. Shang, Y. Ouyang, et al., eScience 2 (2022) 192–200.
[13] P.Y. Ji, J. Fang, Y.Y. Zhang, P. Zhang, J.B. Zhao, ChemElectroChem 4 (2017) 2352–2358.
[14] W. Pu, X. He, L. Wang, C. Jiang, C. Wan, J. Membr. Sci. 272 (2006) 11–14.
[15] W. Xu, X.G. Sun, C.A. Angell, Electrochim. Acta 48 (2003) 2255–2266.
[16] W. Wieczorek, D. Raducha, A. Zalewska, J.R. Stevens, J. Phys. Chem. B 102 (1998) 8725–8731.
[17] Q. Ma, H. Zhang, C. Zhou, et al., Angew. Chem. Int. Ed. 55 (2016) 2521–2525.
[18] P. Lightfoot, M.A. Mehta, P.G. Bruce, Science 262 (1993) 883–885.
[19] J. Cao, D. Zhang, R. Chanajaree, et al., Adv. Powder Mater. 1 (2022) 100007.
[20] Z. Cai, Y. Liu, S. Liu, L. Li, Y. Zhang, Energy Environ. Sci. 5 (2012) 5690–5693.
[21] Q. Liu, G. Yang, X. Li, et al., Energy Storage Mater. 51 (2022) 443–452.
[22] H. Huo, B. Wu, T. Zhang, et al., Energy Storage Mater. 18 (2019) 59–67.
[23] C. Ma, Y. Feng, F. Xing, et al., J. Mater. Chem. A 7 (2019) 19970–19976.
[24] C. Niu, J. Liu, G. Chen, et al., J. Power Source 417 (2019) 70–75.